EPR study on oxygen handling properties of ceria, zirconia and Zr–Ce (1 : 1) mixed oxide samples

A. Martínez-Arias *, M. Fernández-García, C. Belver, J.C. Conesa and J. Soria

Instituto de Catálisis y Petroleoquímica, CSIC, Camino de Valdelatas s/n, Campus UAM, Cantoblanco, 28049 Madrid, Spain
E-mail: amartinez@icp.csic.es

Received 12 November 1999; accepted 28 January 2000

The characteristics of ceria, zirconia and Zr–Ce (1 : 1 molar ratio) samples prepared by using inverse microemulsions have been studied to obtain information on the modifications produced in the oxygen handling properties of the single oxides by the formation of the mixed oxide. The structural characteristics of the samples are compared on the basis of XRD and Raman spectroscopy data, which show that the Zr–Ce sample forms a homogeneous mixed oxide structure corresponding to the (pseudocubic) tetragonal phase t″ while CeO_2 presents, as expected, a cubic fluorite structure and ZrO_2 is formed mainly by a tetragonal phase with only traces of the thermodynamically most stable monoclinic phase. Evaluation by EPR of the type and intensity of superoxide radicals generated upon oxygen adsorption on the outgassed samples reveals a higher surface reducibility in the mixed oxide sample, associated vacancies defects being generated on it in higher amounts and at lower temperatures than on pure ceria. It is also shown that both Ce and Zr ions participate in the oxygen chemisorption process on the mixed oxide sample, actually giving rise to much larger amounts of O_2^-–Zr^{4+} species than the pure ZrO_2 sample; the latter species show a higher thermal stability than O_2^-–Ce^{4+} species.

Keywords: Zr–Ce mixed oxide, CeO_2, ZrO_2, superoxide, oxygen chemisorption, EPR

1. Introduction

Cerium oxide has traditionally been used as a promoting component in three-way catalysts (TWC) employed for the elimination of toxic exhaust gases in automobiles [1]. One of the most important promoting effects of cerium oxide in these catalysts is related to the high oxygen storage capacity (OSC) acquired by the TWC in the presence of this component [2]. This is attributed to the particular ability of CeO_2 to undergo deep and rapid reduction/oxidation cycles according to the reaction $CeO_2 \rightleftharpoons CeO_{2-x} + (x/2)O_2$, which allows this component to interact with reducing or oxidizing components present in the reactant mixtures [2,3], thus broadening the region around the air/fuel stoichiometric value in which the catalysts are effective.

In recent works it has been shown that the OSC can be further enhanced by incorporation of zirconium and formation of mixed Zr–Ce oxides [4,5]. This has been related with the significantly lower temperature, with respect to pure ceria, required for bulk reduction on $Ce_xZr_{1-x}O_2$ systems, a behavior which can be improved further by repeated reduction–oxidation cycles at high temperatures (up to 1273 K) [5]. This, and the more refractory character of the Zr-containing materials, could lead to materials more efficient in those cases where a large sintering of the component can be produced as a consequence of thermal aging [5]. Among the possible phases and compositions of the mixed oxides, it has been observed that the best characteristics for these purposes are achieved for cerium mol% between 50 and 70 and for the pseudocubic phase t″ (having crystallographic tetragonal symmetry but keeping indistinguishable a and c parameters in the fluorite cell) [5].

In spite of the large amount of work dedicated to understand the characteristics of the redox processes taking place in the bulk of these materials [5], little is known on their surface properties; thus, aspects as the kind of surface defects generated upon reduction, or the oxygen handling properties of these, which are most interesting for catalytic purposes, particularly for the comprehension of the light-off behavior of the systems, are unknown yet. In this contribution, we address these points by using an approach similar to that employed in previous works, in which the characteristics of the surface defects generated by outgassing are examined by oxygen chemisorption at low temperature and EPR analyses of the superoxide species so generated [6,7].

2. Experimental

The Zr–Ce mixed oxide sample has been prepared by a coprecipitation method by mixing two microemulsions, one containing an aqueous solution with the same molar fraction of zirconyl nitrate (Aldrich, purity = 99.99%) and cerous nitrate hexahydrate (Aldrich, purity = 99.9%) and the other containing tetramethylammonium hydroxide pentahydrate (supplied by Aldrich). The resulting solid (after centrifugation, decantation and rinsing with methanol) was dried at 383 K for 24 h and calcined in air at 773 K for 2 h (a ramp of 2 K min^{-1} was employed). The so obtained sample will be referred to as ZC; its chemical analysis,

* To whom correspondence should be addressed.

made by ICP-AES, showed $(Ce/Zr)_{at} = 0.52/0.48$, suggesting that a thorough precipitation of both components is achieved. Specific surface area determination by the BET method showed $S_{BET} = 96\ m^2\,g^{-1}$. More details on the preparation and some morphological characteristics of ZC can be found elsewhere [8]. The same method was applied for preparation of single-component zirconium oxide and cerium oxide samples (hereafter referred to as samples Z and C, respectively). After drying and calcination in air at 773 K, samples Z and C showed $S_{BET} = 67$ and $72\ m^2\,g^{-1}$, respectively.

Powder XRD patterns were recorded on a Siemens D-500 diffractometer using nickel-filtered Cu Kα radiation operating at 40 kV and 25 mA, and with a 0.025° step size. Computer fitting was done by using the Winfit! program [9].

Raman spectra were obtained with a Bruker FT-Raman instrument using the 1064 nm exciting line, at a resolution of 4 cm^{-1}, and taking 100 scans for every spectrum.

EPR spectra in the X-band mode ($\nu \approx 9.5$ GHz) were recorded at 77 K with a Bruker ER 200D spectrometer calibrated with DPPH ($g = 2.0036$). Portions of sample (ca. 40 mg) are placed inside a quartz probe cell with greaseless stopcocks, where they can be subjected to outgassing treatments in high-vacuum conditions (ca. $8\times10^{-3}\ N\,m^{-2}$, dynamic vacuum). Oxygen adsorption experiments were carried out by admitting in the cell doses of 70 μmol of O_2 per gram of sample at 77 K, followed by thorough outgassing at 77 K in order to minimize magnetic interactions with non-chemisorbed O_2. Quantitative analysis of the EPR spectra is performed by computer double integration of the spectra and comparison with a copper sulfate standard ($CuSO_4{\cdot}5H_2O$).

3. Results and discussion

3.1. Structural characteristics

Figure 1 shows the X-ray diffractograms of the samples. The main features in the patterns of samples C and ZC are due to reflections indexable according to cubic fluorite-type cells (space group Fm3m) with lattice parameters (calculated using most intense reflections (111) and (220)) increasing with the amount of cerium present in the samples (ZC = 5.280 Å, C = 5.412 Å); these data agree well with values reported for these materials, assuming in the case of sample ZC a molar composition close to 1 : 1 (Ce : Zr) [10,11]. However, it is worth noting that differentiation between the possible cubic and tetragonal phases (the latter belonging to space group $P4_2/nmc$) that could be present in sample ZC is difficult on the basis of XRD only, due to the relative similarity of the a and c lattice parameters of the face-centered fluorite cell expected for these materials for CeO_2 molar fraction below 60%; the displacement of oxygen ions which is responsible for the symmetry decrease is usually difficult to detect, as the X-ray diffractograms are dominated by the scattering of much heavier Zr and Ce atoms [11,12].

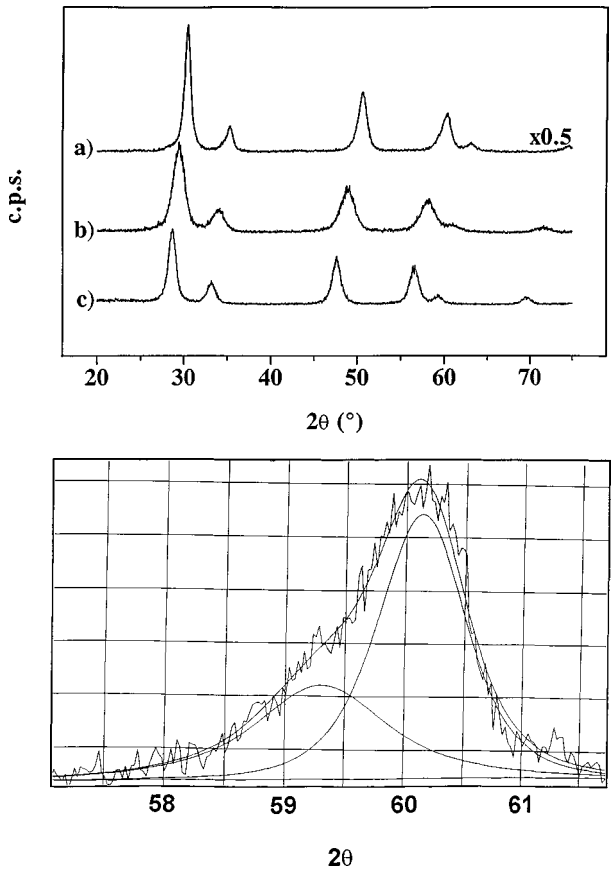

Figure 1. Top: X-ray diffraction patterns of (a) sample Z, (b) sample ZC and (c) sample C. Bottom: fitting of the peak splitting in the zone corresponding to reflection (311) of sample Z.

The diffractogram of sample Z shows shoulders at the low-angle sides of reflections (200) and (311), and at the high-angle side of reflection (220), which suggests that the observed reflections arise from a tetragonal phase. Fitting of the (311) peak (the one having theoretically the highest tetragonal splitting among those showing an appreciable amplitude in the diffractogram obtained) shown in the bottom of figure 1, strongly supports this hypothesis as it yields two components with intensity ratio close to 2 : 1 and $c/a = 1.013 \pm 0.005$, in good agreement with values obtained for the zirconia tetragonal phase [11]. Estimation of the particle size was done by use of the Scherrer equation [10] (111 and 220 reflections being employed) yielding 5.3, 8.5 and 11.7 nm (with an estimated error of ca. 0.3 nm) values for samples ZC, C and Z, respectively. It is worth noting that in the case of sample ZC, for which TEM results are available [8], a good correlation is found between the XRD particle size estimation and the electron microscopy observation. Thus, the observed diffraction linewidth would not be affected strongly (at least for that sample) by strain effects, nor by compositional inhomogeneity, which could lead to a distribution of Ce : Zr ratios and, hence, of lattice parameters.

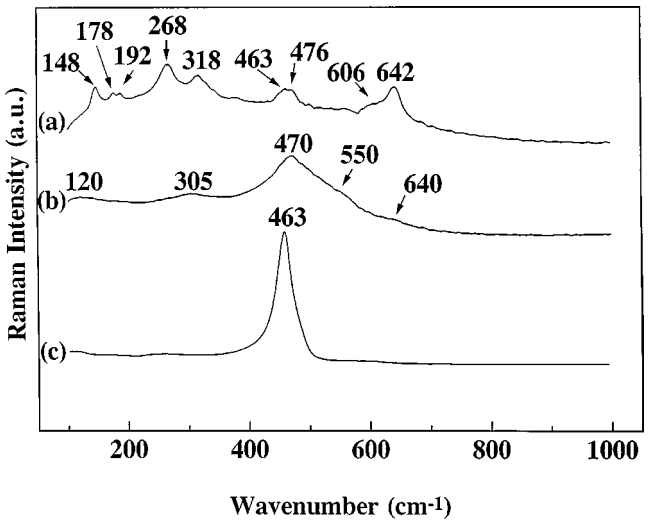

Figure 2. Raman spectra of (a) sample Z, (b) sample ZC and (c) sample C.

Raman spectra of the samples are shown in figure 2. As indicated in earlier work [8], sample ZC exhibits broad bands at ca. 470 cm^{-1} (with shoulders at ca. 550 and 640 cm^{-1}), 305 and 120 cm^{-1}, showing a pattern typical of the presence of the (pseudocubic) tetragonal phase t″ [5,8,13]; for this phase, some of the six Raman-active modes expected for a tetragonal phase [13] become nearly degenerated so that only four bands are detected (the weak shoulder at ca. 640 cm^{-1} being attributed to a localized substitutional defect vibration) [5,13]. In the case of sample Z, the Raman spectrum shows bands attributable to the tetragonal phase (bands at 148, 268, 318, 463, 606 and 642 cm^{-1}) [14], while less intense bands at 178, 192 and 476 cm^{-1}, which coincide with the highest amplitude bands shown by monoclinic zirconia [15], are also observed. The presence in sample Z of a major thermodynamically unstable tetragonal phase can be attributed to the preparation method used here leading to nanosized particles for which the presence of the tetragonal phase is expected below certain critical size value, estimated to be around 17 nm [16]. In the case of sample C, its Raman spectrum shows a single band at 463 cm^{-1}, as expected for its stable cubic fluorite-type structure.

The preceding data show thus that the three samples studied have comparable overall structural characteristics (i.e., only differ in a tetragonality degree and unit cell volume that, respectively, decrease and increase gradually with increasing Ce content). This, together with the similarity of their preparation methods, and the relatively similar high surface areas, makes them suitable for joint comparison and examination of the intrinsic effects of mixed oxide formation on the surface redox chemistry of such materials.

3.2. Minor structural defects detected by EPR on the outgassed samples

Figure 3 shows EPR spectra of the samples subjected to outgassing treatment at $T_v = 473$ K. At this T_v most of the signals observed in the whole range of outgassing T_v examined (373–773 K) are detected. Sample C shows an axial signal A ($g_\perp = 1.964$ and $g_\parallel = 1.941$) along with minor impurity Mn^{2+} features (amounting to ca. 0.1 ppm). Signal A is present in the whole T_v range studied, its intensity increasing slightly with T_v. Sample Z shows for $T_v < 673$ K an axial signal B ($g_\perp = 1.977$ and $g_\parallel = 1.960$), which decreases with increasing T_v; for $T_v \geqslant 573$ K, a weak symmetric signal C at $g = 2.0025$, which grows with T_v, also appears. A more complex situation is observed in the case of sample ZC, since in addition to signals A and C (the latter observed now only for $T_v = 773$ K), new signals A′ ($g_\perp = 1.968$ and $g_\parallel = 1.943$) and B′ ($g_\perp = 1.973$ and $g_\parallel = 1.959$) are observed. Evolution of signals A (or A′) and B′ with T_v is similar to that observed for signals A and B, respectively, in the single-component oxides.

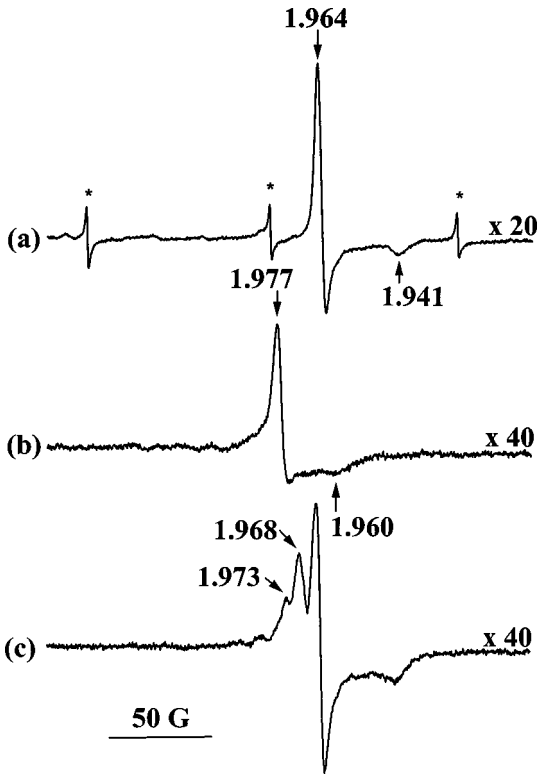

Figure 3. EPR spectra following outgassing at $T_v = 473$ K: (a) sample C, (b) sample Z and (c) sample ZC. $*$ marks indicate lines from a Mn^{2+} impurity.

Signal A is typical of ceria-containing samples. Certain discrepancies exist concerning its assignment. Thus, it has been assigned to unpaired electrons trapped at oxygen vacancies, where these vacancies are stabilized by structural defects or impurities [7]. It has been also proposed that the unpaired electrons might be localized as Ce^{3+} ions in particularly low symmetry positions (in order to justify its detection at 77 K in spite of the low spin relaxation time expected for these ions) or delocalized among ions at the vacancy environment [7,17]. Signal B is similar to that observed previously in other zirconia samples prepared by gel methods and attributed to Zr^{3+} ions [18]. Some of the char-

Table 1
Characteristics of the signals observed by oxygen adsorption at room temperature on the outgassed samples.[a]

Sample	Signal	EPR parameters[b]	Signal intensity[c] (μmol g^{-1})			
			$T_v = 473$ K	$T_v = 573$ K	$T_v = 673$ K	$T_v = 773$ K
C	OC1	$g_{\|} = 2.032$, $g_{\perp} = 2.010$	0.027	–	–	–
	OC2	$g_z = 2.031$, $g_x = 2.017$, $g_y = 2.011$	–	–	–	0.026
	OC3	$g_{\|} = 2.042$, $g_{\perp} = 2.010$	–	0.252	0.351	0.658
	OC4	$g_z = 2.051$, $g_y = 2.009$, $g_x = 2.007$	–	0.108	0.117	0.194
ZC	OC1′	$g_{\|} = 2.034$, $g_{\perp} = 2.011$–2.010	0.248	0.273	0.176	0.184
	OC2′	$g_z = 2.032$–2.031, $g_x = 2.016$–2.017, $g_y = 2.011$	0.016	0.209	0.132	0.100
	OC3′	$g_z = 2.042$, $g_y = 2.010$–2.009, $g_x = 2.009$–2.008	0.173	0.626	0.600	0.651
	OZ′	$g_z = 2.037$, $g_y = 2.009$, $g_x = 2.002$	0.103	0.498	0.556	0.765
Z	OZ	$g_z = 2.040$, $g_y = 2.009$, $g_x = 2.002$	0	0	0.042	0.081

[a] 70 μmol of O_2 per gram of sample are adsorbed at 77 K, followed by outgassing at 77 K, warming to room temperature and, finally, outgassing at room temperature.
[b] Obtained by computer simulations. Axis assignment is based on experiments in which adsorption of ^{17}O-containing oxygen was performed [6]. Axes orientation follows the model of [6,20].
[c] The contribution of every signal in samples C and ZC is obtained by computer simulation.

acteristics of signal B, like the symmetry of the paramagnetic center and linewidth, are similar to those of signal A, while the g values are only a little larger. This suggests that both paramagnetic centers might be of a similar nature, the difference between their g values being related to the changes in the lattice parameters between samples C and Z. In a previous work, it was proposed that defects giving rise to signal C were associated with electrons trapped at oxygen vacancies in the zirconia lattice, being related with the presence of the tetragonal phase of zirconia [19]. For the mixed oxide, formation of new signals A′ and B′, showing parameters similar to those of signals A and B but slightly shifted towards those of signals B and A, respectively, while the lattice parameter of this sample presents an intermediate value between those of the single oxides, suggests for these signals assignments to paramagnetic centers similar to those giving rise to signals A and B in the single oxides but modified by effect of the mixed oxide structure.

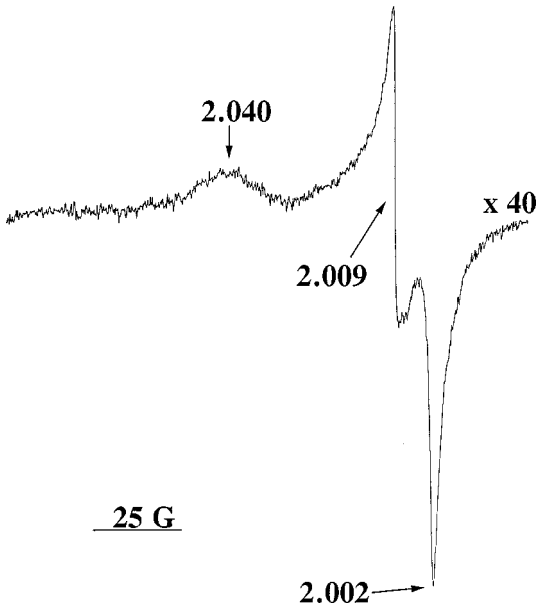

Figure 4. EPR spectrum following oxygen adsorption at $T_a = 373$ K on sample Z outgassed at $T_v = 773$ K.

3.3. EPR study of oxygen adsorption on the outgassed samples

New signals are observed in the EPR spectra following oxygen adsorption on the samples subjected to outgassing at $T_v = 373$–773 K; their characteristics are summarized in table 1, while typical spectra are shown in figures 4–6.

3.3.1. Sample Z

A single signal OZ (figure 4) is observed upon oxygen adsorption at T_a between 77 and 373 K on the outgassed sample Z; its intensity increases with T_v, as shown in table 1, and with T_a, figure 7.

The parameters of signal OZ are typical of ionically bonded O_2^- species; the g_z value agrees with coordination to a tetravalent cation of relatively large radius [20]. Its intensity increase with T_v suggests that formation of the corresponding radicals is related to surface reduction of the sample; they can be attributed to O_2^-–Zr^{4+} species probably formed by oxygen interaction with surface defects generated by the outgassing treatment (like oxygen vacancies) followed by electron transfer from the sample surface. The intensity of signal OZ overwhelms that of signals B or C present prior to oxygen adsorption. This indicates that the electron donor centers are not related to localized paramagnetic Zr^{3+} or trapped electron centers (responsible of signals B or C). These latter localized defective centers present a relatively large stability in this sample, in view that electrons are not easily transferred from them towards oxygen molecules, a result which agrees with previous investigations on other zirconia samples [21]. In a previous work [21], it has been proposed that the electron donor centers could be related with delocalized conduction electrons generated in the semiconductor solid by effect of the partial reduction (in our case, by outgassing) of the sample.

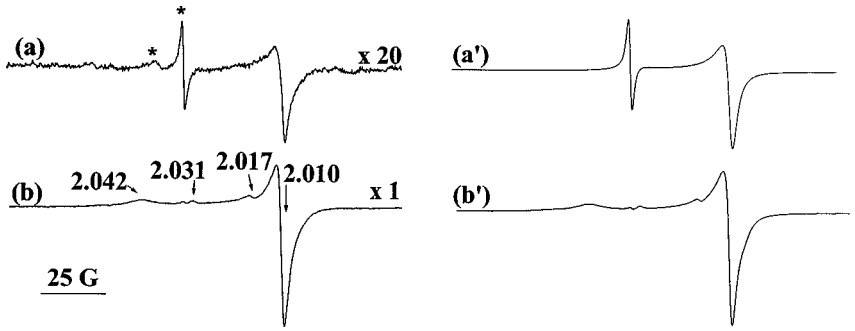

Figure 5. EPR spectra following oxygen adsorption at room temperature and outgassing at room temperature on sample C outgassed at: (a) $T_v = 473$ and (b) 773 K. (a′) and (b′) show computer simulations of the spectra presented in (a) and (b). $*$ marks indicate lines from a Mn^{2+} impurity.

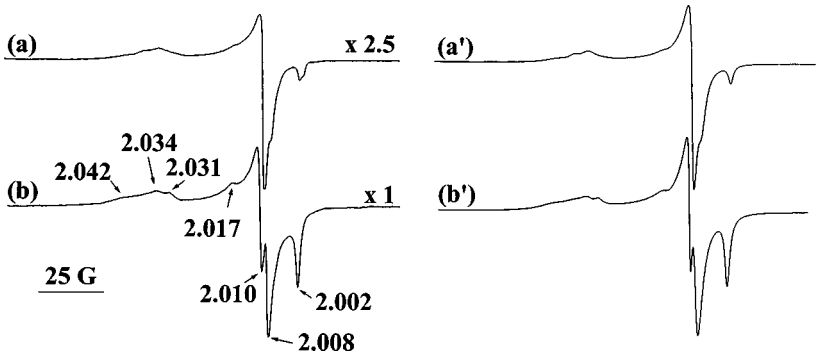

Figure 6. EPR spectra following oxygen adsorption at room temperature and outgassing at room temperature on sample ZC outgassed at: (a) $T_v = 473$ and (b) 773 K. (a′) and (b′) show computer simulations of the spectra presented in (a) and (b). $*$ marks indicate lines from a Mn^{2+} impurity.

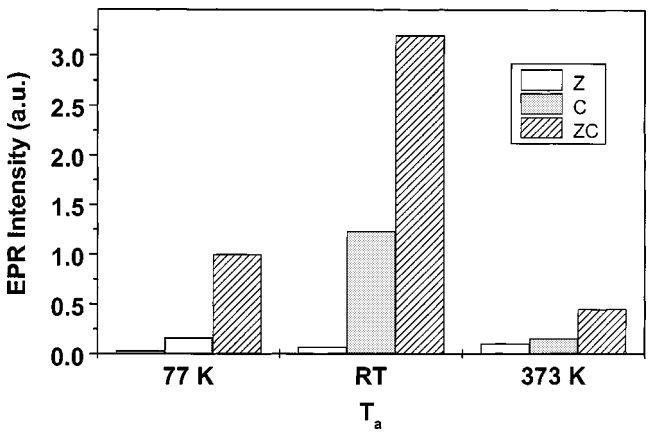

Figure 7. Intensity of superoxide species detected by EPR upon oxygen adsorption on the indicated samples outgassed at $T_v = 773$ K, as a function of the adsorption temperature (T_a).

An earlier work showed $g_z = 2.032$ for O_2^-–Zr^{4+} species formed on zirconia [22]; the substantial difference between the g_z parameter obtained in that work and that observed here ($g_z = 2.040$) for basically the same species could be rooted in differences in the surface structures present in each case, taking into account that the g_z value of these radicals is most sensitive to changes in the configuration of the adsorption center [20,21]. It can be presumed that the O_2^-–Zr^{4+} radical observed here, corresponds to species formed on tetragonal phase particles, while that observed by Setaka and Kwan [22] belongs to species formed on monoclinic ones. This hypothesis is confirmed by recent work in our laboratory [23], in which O_2^-–Zr^{4+} shows $g_z = 2.032$ when oxygen is adsorbed on an outgassed CeO_2/ZrO_2 sample prepared from a monoclinic zirconia support; thus, the higher distortion from purely cubic structure existing in monoclinic phase would be reflected in a smaller g_z value.

3.3.2. Ce-containing samples

Complex spectra formed by the overlapping of different signals are observed when oxygen is adsorbed on samples C or ZC outgassed at $T_v = 373$–773 K. Only a very small signal showing a peak at $g \approx 2.010$, whose parameters cannot be resolved, appears upon O_2 adsorption on any of the samples outgassed at $T_v = 373$ K. For $T_v = 473$–773 K the parameters of the different signals observed have been determined by means of computer simulations (typical examples being shown in figures 5 and 6), taking into account results obtained in previous studies [6,7], as well as the different evolution of the signals as a function of their different ease of formation and stabilities, as will be shown below. These results are collected in table 1.

Assignment of signals type OC (OC1–OC4 and OC1′–OC3′) is based on previous studies of oxygen adsorption on ceria-based materials, in which analyses of the spectra obtained after adsorption of ^{17}O-containing oxygen mixtures was performed [6,7]. All the signals type OC are very similar to those corresponding to superoxide species

adsorbed on cerium ions (formally O_2^-–Ce^{4+}) [6,7], and are then attributed to these species. These signals differ from those corresponding to ionically bonded O_2^- species as they show all of their g values significantly higher than g_e ($g_e = 2.0023$) [20]. This has been attributed to the partially covalent character of the O_2^-–Ce^{4+} bond in these species [7]. A general classification of these signals has been established according to the type of oxygen adsorption center, distinguishing between isolated and associated (anionic) vacancies centers [6]. This distinction was based on the activation conditions required for their generation (higher T_v being needed for generation of the latter) and on the exclusive reactivity for NO reduction (yielding N_2O) of the associated vacancies centers [3,6]. Direct evidence (by STM) of the presence of associated vacancies at the ceria surface is also available [24]. The EPR characteristics of the superoxide species formed on each of these centers was as follows: O_2^- formed on isolated vacancies shows g_x values higher than 2.010 and g_z values lower than 2.037; on the other hand, g_x values lower than ca. 2.009 and g_z values higher than 2.037 were found for O_2^- species formed on associated vacancies centers.

On this basis, signals OC1, OC2, OC1′ and OC2′ can be attributed to O_2^-–Ce^{4+} species formed on isolated vacancy centers while signals OC4 and OC3′ can be attributed to O_2^-–Ce^{4+} species formed on associated vacancies centers. Some doubts can exist in respect to attribution of signal OC3 on the basis of these arguments. The similarity of its parameters with those of signal OC3′ (in particular, the g_z value) suggests that both centers might be of a similar kind, the small differences between their g_x values being then probably due to the presence of Zr in the ZC sample. In a previous work, the differences between superoxide species formed on associated vacancies (signals OC3 – or OC3′ – and OC4) has been attributed, mainly on the basis of the activation temperature required for their generation, to the relatively higher degree of coordinative unsaturation of the adsorption centers giving rise to signal OC4 [6].

Table 1 shows important differences among the O_2^-–Ce^{4+} species formed on samples C and ZC. First, an easier formation of oxygen vacancies, without formation of centers with the higher unsaturation degree (giving rise to signal OC4), is observed for ZC. In second place, isolated and associated oxygen vacancies coexist for sample ZC. These characteristics indicate a more homogeneous distribution of the oxygen vacancies in sample ZC, as should be expected for a sample with higher oxygen mobility [5].

Signal OZ′, which presents parameters typical of ionically bound O_2^- species, similar to those shown by signal OZ, must be attributed to O_2^-–Zr^{4+} species. Noteworthy, the g_z value of signal OZ′ (2.037) is lower than that of signal OZ (2.040). Since distortion from the cubic symmetry is here even lower than in sample Z, this difference in g_z must be attributed to differences in the environment of the adsorption site in each of the cases due to the presence of a mixed oxide surface for sample ZC.

3.4. Ease of formation and stability of the superoxide species

Figure 7 shows the overall intensity of superoxide species formed upon O_2 adsorption on the samples outgassed at $T_v = 773$ K, as a function of the adsorption temperature (T_a), up to $T_a = 373$ K (in all cases, the spectra were recorded at 77 K). While samples C and ZC show a maximum at $T_a =$ RT, sample Z shows the highest intensity at $T_a = 373$ K.

These results reveal that the generation of superoxide radicals in these samples is slightly activated [21]. For the cerium-containing samples, only signals due to O_2^-–Ce^{4+} species formed on isolated vacancies are observed for $T_a = 77$ K, while all of the signals appearing in these samples show their maximum intensity for $T_a =$ RT. This indicates that, within the cerium-containing samples, a higher activation energy is involved in the oxygen chemisorption process on associated vacancies (for both samples C or ZC) or on Zr ions (for sample ZC) than on isolated vacancies.

On the other hand, considering the general scheme accepted to be followed in the oxidation process of this kind of materials [20]: $O_2 \rightarrow O_2^- \rightarrow O_2^{2-} \rightarrow 2O^- \rightarrow 2O^{2-}$, the superoxide signal intensity decrease observed for $T_a >$ RT in samples ZC or C must be attributed to a thermally induced further evolution in the oxidation process leading to formation of (diamagnetic) peroxide or oxide anions. This is confirmed by experiments of oxygen adsorption (at RT) on the samples treated at $T_a = 373$ K, which showed no recovery of the superoxide species.

Another interesting result concerns comparison of the stability of species O_2^-–Ce^{4+} and O_2^-–Zr^{4+} in sample ZC. Thus, by outgassing at 373 K the sample that has been in contact with oxygen at $T_a =$ RT, almost all O_2^-–Ce^{4+} species are eliminated but signal OZ′ remains (figure 8); this reveals the higher stability of O_2^-–Zr^{4+} species, which may be related to the smaller ionic radius of Zr^{4+}. This could have implications on the reactivity of these samples, as the equilibrium concentration of superoxide species in the Zr–Ce mixed oxide sample could be higher than in

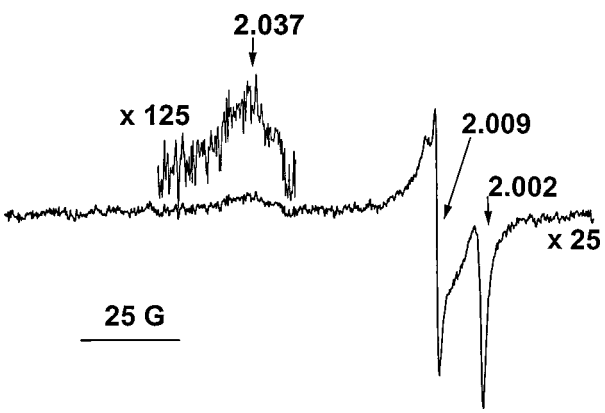

Figure 8. EPR spectra of sample ZC after oxygen adsorption at room temperature on the sample outgassed at $T_v = 773$ K (spectrum shown in figure 6(b)) and subsequent outgassing at 373 K.

CeO_2 as a consequence of their stabilization as O_2^-–Zr^{4+} species.

3.5. Differential characteristics of the mixed oxide with respect to the single oxides

A consequence of the formation of the mixed oxide concerns the higher amount of both O_2^-–Ce^{4+} and O_2^-–Zr^{4+} species formed in the mixed oxide than in the corresponding single component oxides (table 1). Considering that formation of the superoxide species involves electron transfer from the reduced sample surface, the intensity of superoxide species (in the respective maximum for each of the samples) gives in principle a measure of the degree of surface reduction achieved in each case. Thus, the results of figure 7 reveal the higher surface reducibility of the mixed oxide sample with respect to the single component oxides. It is also interesting to note that not only cerium but also zirconium cations are involved in the oxygen chemisorption, a significant amount of superoxide radicals being formed on the latter (figure 7). Considering the difficulty to reduce Zr^{4+} cations, as evidenced by XANES in previous works on other mixed oxide samples [5,25], the most likely explanation to account for this result is the existence of oxygen transfer phenomena by which oxygen molecules activated at cerium cations are transferred to close cus oxidized zirconium cations. It must be considered however that since, as pointed out above, there exist doubts on the nature of the donor centers responsible for the formation of O_2^-–Zr^{4+} species, it cannot be discarded that the higher amount of these radicals in the mixed oxide sample would be related to direct oxygen interaction with cus surface zirconium cations favored by a promoted generation of surface vacancies in the coordinative environment of such cations, along with the higher reducibility shown by this sample. Further experiments are certainly needed to get a deeper knowledge of this process.

The easier surface reducibility of the mixed oxide sample is also revealed by the higher facility for generating associated vacancies on the mixed oxide sample, as indicated by formation of a significant amount of signal OC3′ already at $T_v = 473$ K in sample ZC while $T_v \geqslant 573$ K is required to generate similar defects on sample C (table 1). A similar result was obtained in a previous work comparing sample ZC with a high surface area commercial ceria sample [8].

In the same sense, the decrease of signal OZ′ (by a factor of ca. 5) when going from $T_a =$ RT to $T_a = 373$ K in sample ZC, which contrasts with the growth of signal OZ in sample Z (figure 7), indicates that a more pronounced reduction of the O_2^- ions bonded to Zr cations is produced in the mixed oxide sample. This indicates that the activation energy for the electron transfer process is higher in sample Z than in sample ZC, which might be a consequence of the higher reduction degree achieved by the mixed oxide.

4. Conclusions

- Surface reduction by outgassing is favored in the Zr–Ce mixed oxide with respect to the single component zirconium or cerium oxides, as evidenced by the higher intensities of O_2^-–Ce^{4+} and O_2^-–Zr^{4+} obtained upon oxygen adsorption in the mixed oxide. A relatively high amount of O_2^-–Zr^{4+} species is formed in the mixed oxide, which could be related to the existence of phenomena involving transfer of oxygen species from more (cerium) to less (zirconium) reducible ions.
- In the Zr–Ce mixed oxide, Zr ions present a different surface local structure than in the ZrO_2 sample or in monoclinic zirconia, as evidenced by the different g_z value shown by the O_2^-–Zr^{4+} species in each of the samples.
- The different thermal behavior of the various superoxide species reveals differences in the activation energies required for their formation as well as in the redox properties of the surface centers where they are created. Results in the mixed oxide sample reveal a higher stability of O_2^-–Zr^{4+} with respect to O_2^-–Ce^{4+} species.

Acknowledgement

Thanks are given to the CAICYT (No. MAT 97-0696-C02-01) and the Comunidad de Madrid (Project No. 06M/085/96) for financial help. AMA and MFG greatly acknowledge the Comunidad de Madrid and the CSIC, respectively, for postdoctoral grants or contracts under which this work was carried out.

References

[1] R.M. Heck and R.J. Farrauto, *Catalytic Air Pollution Control; Commercial Technology* (Van Nostrand Reinhold, New York, 1995).
[2] H.C. Yao and Y.F. Yu Yao, J. Catal. 86 (1984) 254.
[3] A. Martínez-Arias, J. Soria, J.C. Conesa, X.L. Seoane, A. Arcoya and R. Cataluña, J. Chem. Soc. Faraday Trans. 91 (1995) 1679.
[4] G. Vlaic, R. Di Monte, P. Fornasiero, E. Fonda, J. Kašpar and M. Graziani, J. Catal. 182 (1999) 378.
[5] J. Kašpar, P. Fornasiero and M. Graziani, Catal. Today 50 (1999) 285, and references therein.
[6] J. Soria, A. Martínez-Arias and J.C. Conesa, J. Chem. Soc. Faraday Trans. 91 (1995) 1669.
[7] A. Martínez-Arias, J.M. Coronado, J.C. Conesa and J. Soria, in: *Rare Earths*, eds. R. Sáez Puche and P. Caro (Complutense, Madrid, 1997) p. 299.
[8] A. Martínez-Arias, M. Fernández-García, V. Ballesteros, L.N. Salamanca, J.C. Conesa, C. Otero and J. Soria, Langmuir 15 (1999) 4769.
[9] Program Winfit!, v. 1.2, © S. Krumm; available at http://www.geol.uni-erlangen.de
[10] M.H. Yao, R.J. Baird, F.W. Kunz and T.E. Hoost, J. Catal. 166 (1997) 67.
[11] M. Yashima, K. Morimoto, N. Ishizawa and M. Yoshimura, J. Am. Ceram. Soc. 76 (1993) 1745.
[12] F. Sánchez-Bajo, I. Cachadiña, J.D. Solier, F. Guibertau and F.L. Cumbrera, J. Am. Ceram. Soc. 80 (1997) 232.

[13] M. Yashima, H. Arash, M. Kakihana and M. Yoshimura, J. Am. Ceram. Soc. 77 (1994) 1067.
[14] D.-J. Kim, H.-J. Jung and I.-S. Yang, J. Am. Ceram. Soc. 76 (1993) 2106.
[15] V.G. Keramidas and W.B. White, J. Am. Ceram. Soc. 57 (1974) 22.
[16] A. Chaterjee, S.K. Pradhan, A. Datta, M. De and D. Chakravorty, J. Mater. Res. 9 (1994) 263.
[17] M. Che, J.F.J. Kibblewhite, A.J. Tench, M. Dufaux and C. Nacache, J. Chem. Soc. Faraday Trans. I 69 (1973) 857.
[18] H. Liu, L. Feng, X. Chang and Q. Xue, J. Phys. Chem. 99 (1995) 332.
[19] M.J. Torralvo, M.A. Alario and J. Soria, J. Catal. 86 (1984) 473.
[20] M. Che and A.J. Tench, Adv. Catal. 32 (1983) 1.
[21] M. Anpo, M. Che, B. Fubini, E. Garrone, E. Giamello and M.C. Paganini, Topics Catal. 8 (1999) 189.
[22] M. Setaka and T. Kwan, Bull. Chem. Soc. Jpn. 43 (1970) 2727.
[23] A. Martínez-Arias, unpublished results.
[24] H. Nöremberg and G.A.D. Briggs, Phys. Rev. Lett. 79 (1997) 4222.
[25] G. Ranga Rao, P. Fornasiero, R. Di Monte, J. Kašpar, G. Vlaic, G. Balducci, S. Meriani, G. Gubitosa, A. Cremona and M. Graziani, J. Catal. 162 (1996) 1.